Analyst

ROYAL SOCIETY OF CHEMISTRY

PAPER

View Article Online
View Journal | View Issue

Cite this: *Analyst*, 2023, **148**, 573

A dummy molecularly imprinted ratiometric fluorescence nanosensor for the sensitive detection of guanidyl-microcystins in environmental water†

Ping Li,[a] Hao Fu,[a] Zhenyu Bai,[a] Xiaoyang Feng,[a] Ji Qi,[b] Xingliang Song,*[a] Xueping Hu *[a] and Lingxin Chen [b,c]

An effective strategy is proposed to construct a highly sensitive ratiometric fluorescence sensing platform for microcystins (MCs) based on a dummy molecularly imprinted polymer using metformin as a template. The imprinted nanohybrids of carbon dots (CDs) combined with fluorescein isothiocyanate (FITC) are synthesized (CDs-FITC-SiO_2@MIP), in which the CDs and FITC serve as assisted response signals and reference enhancement signals, respectively. Metformin can be used as a dummy template for MCs due to its partially similar molecular fragments to MCs that can form a specific recognition site cavity. MCs can simultaneously induce an obvious fluorescence quenching effect for the CDs and a reference fluorescence enhancement for FITC-SiO_2, enabling ratiometric fluorescence detection of MCs. Thus, CDs-FITC-SiO_2@MIP used as a signal probe has favorable sensitivity, stability, and selectivity. More importantly, a good linear relationship between the fluorescence intensity ratio ($I_{620/450}$) and the concentration of MCs in the range of 0.5–500 μg L^{-1} is obtained with a LOD of 0.013 μg L^{-1} and 0.022 μg L^{-1} for MC-RR and MC-LR, respectively, under the optimum conditions. This method has great application potential in water quality monitoring by using CDs-FITC-SiO_2@MIP as a promising candidate for monitoring MCs in complex systems.

Received 25th November 2022,
Accepted 14th December 2022

DOI: 10.1039/d2an01928k

rsc.li/analyst

Introduction

With the aggravation of worldwide environmental water eutrophication, the frequency of algal bloom events is increasing gradually.[1] Among them, some algae produce algal toxins that cause serious harm to ecosystems and human health by polluting water.[2] Microcystins (MCs) are typical algal toxins with a cyclic heptapeptide structure produced by cyanobacteria. They have a strong carcinogenic effect on humans and are potent toxins throughout the food chain.[3] Furthermore, MCs can still retain certain activity even at a high temperature of 300 °C.[4,5] Among various isomers of MCs, MC-RR and MC-LR are receiving extensive attention due to their toxicity and frequent presence. The content of MCs has been restricted to <1 μg L^{-1} by the World Health Organization (WHO) in drinking water.[6] Therefore, sensitive and selective detection of MCs is essential.

Some biochemical and instrumental methods have been developed to detect MCs, including liquid chromatography,[7] enzyme-linked immunosorbent assays,[8] electrochemical analysis,[9] protein phosphatase inhibition test,[10] colorimetric inhibition test,[11] capillary electrophoresis,[12] *etc.*[13,14] However, these methods have associated problems of high cost and slow detection speed due to the materials used and the enrichment process. The detection of trace MCs is still challenging in environmental samples. So, developing effective and rapid methods for detecting trace MCs is imperative.

The innovative and low-cost molecularly imprinted polymer (MIP)-based fluorescence sensing method is highly promising for the sensitive and selective detection of MCs. MIPs offer the benefits of higher selectivity, good chemical stability, easy preparation and low cost and work as an artificial antibody being widely available for chemical sensing.[15,16] Qi *et al.*[17] reported a carbon dot molecularly imprinted fluorescence sensor for determining MC-LR with high sensitivity and selectivity. The purification of MCs is problematic, resulting in

[a]*School of Chemistry and Chemical Engineering, Linyi University, Linyi, 276005, P. R. China. E-mail: xlssong@yeah.net, xuephu@yeah.net*
[b]*CAS Key Laboratory of Coastal Environmental Processes and Ecological Remediation, Research Center for Coastal Environmental Engineering and Technology, Yantai Institute of Coastal Zone Research, Chinese Academy of Sciences, Yantai 264003, China*
[c]*School of Pharmacy, Binzhou Medical University, Yantai, 264003, China*

† Electronic supplementary information (ESI) available: The binding explanation; optimized conditions; characterization section; the UV-vis, fluorescence and MS spectra; selectivity parameters and zeta potential; molecular structure and charge distribution; Mott–Schottky diagram; detection of the actual water sample; a performance comparison table of the sensor with other sensors. See DOI: https://doi.org/10.1039/d2an01928k

the difficulty of obtaining sufficient standard reagents for MCs.[18] Fortunately, imprinting with a dummy template provides an opportunity to reduce costs. A segment of the MC molecule is used instead of MCs as templates for synthesizing MIPs. MIPs synthesized using a dummy template also have a recognition effect on MCs. Mbukwa *et al.*[19] successfully fabricated MIPs using L-arginine for imprinting with a dummy template and the MIPs finally showed good performance in the determination of MCs. Li *et al.*[20] proposed a dual-fragment dummy template imprinting strategy based on Mn–ZnS quantum dots combined with room temperature phosphorescence to detect MCs homologues. Furthermore, the MIP-based ratiometric fluorescence sensing detection has attracted significant attention[21–25] because of its high sensitivity, fast response, facile sample pretreatment, and anti-interference. Compared with a single fluorescence sensor, the ratiometric fluorescence sensor has the ability to perform self-correction by multiple fluorescence emissions.[26–30] Generally, constant fluorescence emission is required as a reference signal in ratiometric fluorescence sensing. In addition, the absence of constant fluorescence emission is also an important type of ratiometric fluorescence sensing. For example, in such systems, the target can cause the enhancement of one fluorescence emission and the quenching of the other simultaneously. The advantages are increased analytical sensitivity and reliability in MC detection. Therefore, to our knowledge, we are the first to develop the MIP-based dual responsive ratiometric fluorescence sensing mode for detecting MCs. In previous studies, it was very difficult to detect two or more components in the same sample at the same time. In order to solve this problem, this study has tried its best to achieve the detection of two mixed components.

Herein, an innovative molecular imprinting ratiometric fluorescence sensor was developed. Based on carbon dots (CDs) and fluorescein 5(6)-isothiocyanate (FITC)-modified silicon spheres, the MIP layer was synthesized using metformin (analogs of MCs) as a dummy template by the sol–gel method. In this sensor, MCs can simultaneously induce fluorescence quenching of CDs and fluorescence enhancement of FITC after selective recognition by MIP layers in the presence of MCs. Therefore, the developed sensor was ultrasensitive and highly selective for detecting MCs. The sensor has good optical properties, water solubility, low toxicity, low cost, and environmental friendliness. This method has significant application prospects for the sensitive and selective determination of trace MCs in environmental water.

Experimental

Chemicals and instruments

All reagents and chemicals were of analytical grade. Tetraethyl orthosilicate (TEOS), metformin, 3-aminopropyl triethoxysilane (APTES), ammonium persulfate (APS), *N*,*N*-dimethylimidodicarbonimidicdiamide, Triton X-100, *N*-(β-aminoethyl)-γ-aminopropyl methyldimethoxysilane (AEAPMS) and fluorescein 5(6)-isothiocyanate (FITC) were purchased from Shanghai Macklin Biochemical Co., Ltd (Shanghai, China). Ammonia solution, petroleum ether, ethanol, and citric acid were obtained from Tianjin Hengxing Chemical Preparation Co., Ltd (Tianjin, China). Microcystin-RR and Microcystin-LR were obtained from Taiwan Algal Science Inc. Ultrapure water was treated with secondary water and used to prepare solutions.

CD synthesis utilized a hydrothermal kettle magnetic stirring heating jacket (HWJB-2100M). The morphology of the novel CDs-FITC-SiO_2@MIP was characterized by transmission electron microscopy (TEM) measurements and scanning electron microscopy (SEM) (SU8010, Hitachi, Japan). And the TEM elemental mapping of CDs-FITC-SiO_2@MIP was characterized using a JEM-2100 High Resolution TEM (Beijing, China). The nanoparticle size was measured using a Marvin Zetasizer Nano ZS90 nanoparticle size potential analyzer (Malvern, Britain). FTIR absorption was recorded using a FTIR-650 purchased from Gang Dong Scientific and Technical Co., Ltd. The Mott–Schottky electrochemical test method was carried out using a CHI660E (Shanghai China). The concentrations of MCs in the real water samples were determined by using high performance liquid chromatography-tandem mass spectrometry (HPLC-MS, 1290-6495, Agilent, USA). All fluorescent emission spectra were measured on a Cary Eclipse (Beijing, China).

Synthesis of CDs and fluorescently labeled silica spheres

CDs were prepared following the previously reported method with slight changes.[31] Firstly, 0.4 g of citric acid was dissolved in 15 mL AEAPMS and degassed with nitrogen for about 15 min. The solution was loaded into a 50 mL Teflon-lined stainless steel autoclave and then heated at 230 °C in a HWJB-2100M for about 2 h. The reaction solution was filtered using a 0.22 μm microfiltration membrane. After filtration, the filtered liquor was washed three times with petroleum ether. The CDs were dispersed in ethanol for later use.

Fluorescently labeled silica spheres were also prepared according to the method reported in the literature.[32] 4.3 mg FITC was dissolved in 10 mL water and stirred evenly using a magnetic stirrer at room temperature. The subsequent addition of 100 μL APTES and stirring at a constant temperature for 24 h afforded the FITC-APTES precursor. 1.80 mL Triton X-100, 2 mL hexyl alcohol, and 8 mL cyclohexane were mixed at room temperature by magnetic stirring for 30 min to provide a uniform mixture. Next, a certain amount of the FITC-APTES precursor was added as a dispersed phase, and the stirring was continued, forming a stable oil–water emulsion. 100 μL TEOS was slowly and uniformly dripped into the above microemulsion system. After stirring for 30 min at 25 °C, 60 μL ammonia (25%) was added as the catalyst, and stirring was continued at a constant temperature for 24 h. Afterward, 10 mL of acetone solution was added for demulsification. After high-speed centrifugation, the product was washed with absolute ethanol and ultrapure water several times, vacuum dried, and stored.

Preparation of the molecular imprinting ratiometric fluorescent sensor

CDs-FITC-SiO_2@MIP were prepared by a typical sol–gel process.[33] Metformin (200 mg) and CDs were added to ethanol (40 mL) in a 100 mL beaker. To the above solution, a certain volume of FITC-SiO_2 composite nanoparticle solution dissolved in ethanol, APTES (350 μL), TEOS (1.5 mL) and ammonia water (800 μL) was added, and the resulting mixture was stirred continuously for 24 h at 25 °C. The product was then collected by centrifugation, and the template molecules in the imprinted cavity were extracted with ethanol and acetonitrile (v/v = 8 : 2), until the template molecules could not be detected from the washing solvent using a UV spectrometer. The CDs-FITC-SiO_2@MIP were dried overnight in a vacuum chamber at 60 °C. NIPs were prepared without the metformin template.

Analytical procedures

The dried molecularly imprinted coating powder was dissolved in normal saline to prepare the molecularly imprinted coating working solution (400 μg mL^{-1}). 3 mL of the working solution was transferred into the test tube, and to this, a series of microcystin solutions (0.5 mL) of different concentrations were added. During the fluorescence analysis, the excitation wavelength was 310 nm, the excitation and emission slit width was 10 nm, and the emission was recorded in the wavelength range of 400–700 nm.[34] Fluorescence intensities of F_{450} and F_{620} were recorded at 450 and 620 nm, respectively. The fluorescence ratio was calculated according to the following formula (1):

$$I_{620/450} = \frac{(F_{620}/F_{450})}{(F_{620}/F_{450})_0}, \quad (1)$$

where $(F_{620}/F_{450})_0$ represents the ratio of F_{620} and F_{450} without microcystin, and (F_{620}/F_{450}) represents their ratio in the presence of microcystins.

Selectivity experiments

Different types of MCs such as MC-RR, MC-LR, MC-YR, and MC-LY, as well as two other competitors, domoic acid and aflatoxin, were used to study the selectivity of CDs-FITC-SiO_2@MIP. According to the report of Özgür *et al.* on the selective detection of melatonin,[35] we configured these substances to be measured at a concentration of 500 μg L^{-1} and then subjected them to a reaction with CDs-FITC-SiO_2@MIP to measure the fluorescence intensity. Then, these results were normalized to easily determine the changes in the fluorescence intensity. The normalized value refers to the difference in the fluorescence ratio of CDs-FITC-SiO_2@MIP before and after the addition of microcystins to the fluorescence reaction. The selectivity constant (k), relative selectivity constant (k'), and IF (imprinting factor) are calculated using the following equations:

$$k = \frac{I_{620/450\,\mathrm{MIP\,objective}}}{I_{620/450\,\mathrm{MIP\,competitive}}}, \quad (2)$$

$$k' = \frac{k_{\mathrm{MIP}}}{k_{\mathrm{NIP}}}, \quad (3)$$

$$\mathrm{IF} = \frac{I_{620/450\,\mathrm{MIP}}}{I_{620/450\,\mathrm{NIP}}}, \quad (4)$$

where k is the selectivity of CDs-FITC-SiO_2@MIP to target competitors. The competitors chose domoic acid with the lowest fluorescence response to CDs-FITC-SiO_2@MIP. k' is the relative selectivity constant of CDs-FITC-SiO_2@MIP against CDs-FITC-SiO_2@NIP. The imprinting factor (IF) is the ratio of specific to nonspecific binding of each compound.

Real sample analysis

The practical applicability of the CDs-FITC-SiO_2@MIP for microcystin detection in complex water samples was examined. For the experiments, the lake water of Binhai Lake in summer on the campus of Linyi University was used. The water samples were pretreated by the following method before removing the actual sample matrix. In a solid phase extraction device, the Binhai Lake water was filtered using a C18 column. After filtration, the MCs were washed with methanol and dissolved in methanol, and then evaporated in a water bath at 60 °C. The pre-treatment measurement of the actual samples is as follows. Tap water samples were obtained from Linyi University after 5 min of flow. To remove the suspended particles, all water samples were centrifuged before use and then filtered using a 0.22 μm microfiltration membrane. The real samples were analyzed by the standard addition method and standard recovery method.

Results and discussion

Construction and the possible mechanism of detecting MCs using the CDs-FITC-SiO_2@MIP sensor

Fig. 1 illustrates the construction of the CDs-FITC-SiO_2@MIP sensor and the possible mechanism for the ratiometric fluorescence detection of MCs. As evident from Fig. 1, CDs and FITC-SiO_2, used to prepare MIPs, provide blue and yellow-green fluorescence, respectively. Since metformin contains guanidine groups with similar structures to microcystins (the similar chemical structures are shown in Fig. S1),† metformin is selected as the dummy template. Both metformin and APTES have $-NH_2$, and they can form hydrogen bonds through nitrogen atoms with strong electronegativity and hydrogen atoms on $-NH_2$[17] (Fig. S4†). The molecular charge distribution of metformin was simulated using Gaussian 98, as can be seen from Fig. S2;† the combination of APTES and metformin was also well demonstrated using UV spectra and zeta potentials (see ESI SI.1† for details). The CDs-FITC-SiO_2@MIP sensor was constructed by anchoring a metformin imprinted layer and CDs on the surface of SiO_2 nanoparticles, using metformin, APTES, TEOS, and $NH_3{\cdot}H_2O$ as the dummy imprinting template, functional monomer, cross-linker, and catalyst, respectively. After the template removal, CDs-FITC-SiO_2@MIP, similar

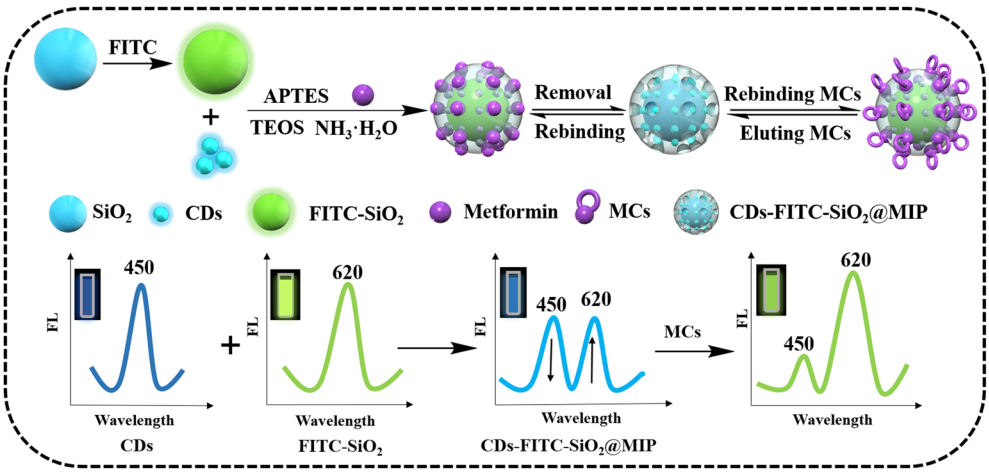

Fig. 1 Schematic illustration of the construction procedure and possible mechanism of the CDs-FITC-SiO_2@MIP sensor to detect MCs.

to microcystin fragments in terms of the functional groups, was successfully obtained (Fig. 1). Upon excitation at only a single wavelength of 310 nm, the constructed CDs-FITC-SiO_2@MIP sensor showed bimodal emission at 450 and 620 nm (Fig. 1). Upon adding MCs, the CDs-FITC-SiO_2@MIP sensor with the tailor-made binding cavities captured them and rebound with them, and the nearby blue emission of the CDs was gradually quenched by the MC bonding at different rates. Simultaneously, the yellow-green fluorescence of FITC was enhanced.

The possible mechanism by which MCs reduce the fluorescence of CDs in the CDs-FITC-SiO_2@MIP fluorescent sensor is described below. Generally, the photoinduced electron transfer (PET) mechanism[36,37] is used to explain the CD fluorescence quenching induced by MCs. In order to evaluate the electron transfer in the two energy transfer systems, CDs and MCs, we need to determine their energy level positions. So, we first determined the position of the lowest unoccupied orbital (LUMO) of the CDs and MCs. We used the Mott–Schottky electrochemical test method.[38] In fact, the LUMO potential is equal to the flat band potential in the Mott–Schottky electrochemical test method, and we can determine the LUMO potential using this flat band potential. The tests for this experiment were carried out at 1000 Hz frequency. After a series of processes, the Mott–Schottky diagram was finally obtained, as shown in Fig. S5A and B.† The value obtained by the intersection of the tangent and abscissa is the flat band potential value. The LUMO potentials of CDs and MC-RR are −1.22 eV and −1.7 eV, respectively (relative to Ag/AgCl, pH = 7), which are usually converted into the potential relative to the standard hydrogen electrode. After conversion, the LUMO potentials of CDs and MC-RR were −0.6 eV and −1.08 eV (Fig. 2), respectively (pH = 0 relative to the NHE). The band gap value was obtained by determining the relationship between the absorption coefficients of the UV-Vis absorption spectra of the CDs and MC-RR and the optical band gap, as shown in Fig. S5C and D.† By combining the value of the LUMO potential and

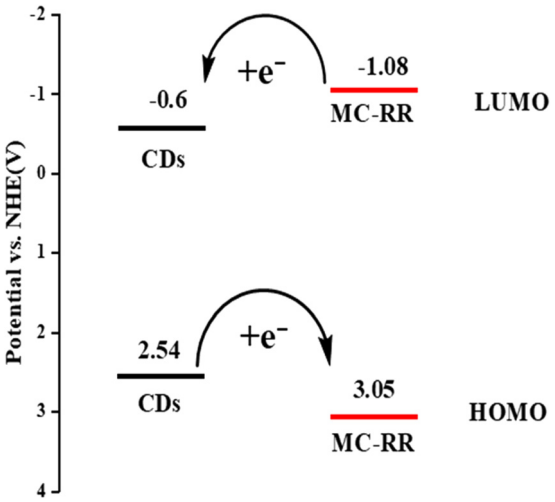

Fig. 2 The energy level diagram of the CDs and MC-RR.

the band gap value, the value of the highest occupied orbital (HOMO) can be obtained. We found that the HOMO potential of the CDs and MC-RR were 2.54 eV and 3.05 eV (Fig. 2), respectively (pH = 0 relative to the NHE). The quenching effect is mainly attributed to the electron transfer between the –NH– of the CDs and the C═O bond of the MC frontal orbital. The C═O group serves as the acceptor of electrons, and –NH– as the donor of electrons due to its strong electron adsorption capacity. In particular, under UV excitation, the electrons on –NH– move from the HOMO to LUMO. Then the MC and APTES compound form hydrogen bonds, which reduces the total energy of the MIP system and makes the LUMO energy level on the C═O bond lower than that of –NH–. Thus, the C═O electron first returns to the HOMO, occupying the original molecular orbital of –NH–, leading to an incomplete electron transition of –NH–. Finally, the fluorescence quenching of CDs occurs. The possible mechanism of FITC fluorescence

enhancement by MCs in the CDs-FITC-SiO_2@MIP fluorescent sensor is due to that the hydrophobic conditions can enhance the fluorescence intensity of FITC. When MCs combine with the sensor, the interaction interface generating the hydrophobic conditions is conducive to the emission of FITC,[39–41] which causes a gradual increase in the fluorescence intensity of FITC during the formation of the complex.

Characterization of the CDs-FITC-SiO_2@MIP sensor

The morphology of the CDs was characterized by TEM. The image of the CDs showed a diameter of about 10 nm (Fig. 3A). The morphology of the fluorescently labeled silica spheres was investigated by SEM, which showed regular and uniform spheres of FITC-SiO_2 nanoparticles (Fig. 3B). Then, the particle size distribution was measured using a laser particle size distribution instrument. The diameter of the FITC-SiO_2 nanoparticles was about 500 nm (Fig. 3C). Further, we analyzed the element distribution of the FITC-SiO_2 nanoparticles using the high-angle annular dark-field images of TEM (Fig. 3D and E), which showed the distribution of Si, O, S, and N elements on the surface of the spherical nanoparticles, confirming the successful preparation of FITC-SiO_2 nanoparticles. The TEM morphological analysis of the CDs-FITC-SiO_2@MIP revealed the adhesion of the molecularly imprinted composite nanoparticles due to the formation of the imprinted layer, indicating the successful synthesis of CDs-FITC-SiO_2@MIP nanoparticles (Fig. 3F).

Fig. 4 shows the FT-IR spectra of FITC-SiO_2, CDs, CDs-FITC-SiO_2@MIP, and CDs-FITC-SiO_2@NIP. In the FT-IR spectrum of the CDs (Fig. 4A), the wide peak at 3400 cm^{-1} belongs to the secondary amide nitrogen hydrogen stretching vibration, while the peak at 1650 cm^{-1} is assigned to the characteristic absorption peak of the CO–NH bond, and the peak at 1465 cm^{-1} results from the secondary amide nitrogen hydrogen bending and carbon–nitrogen stretching. The presence of these peaks reveals the formation of amide bonds, which is the most typical feature indicating the successful synthesis of the CDs. The strong absorption peaks observed near 469 cm^{-1} and 1090 cm^{-1} are the characteristic vibration peaks of silicon oxide, corresponding to the asymmetric bending vibration and stretching vibration of the Si–O–Si bond, respectively. An additional peak at 1555 cm^{-1} is also evident, ascribed to the N–H bending vibration.[42] Thus, the FT-IR results prove that the amino functional group is successfully modified into silica materials, which further indicates that FITC is connected to the silica nanoparticles through covalent bonds by coupling with APTES. The above synthesis process was confirmed by the UV-Vis absorption spectra and fluorescence spectra (Fig. S5†). The UV-Vis spectrum of the CDs showed characteristic absorption peaks at 349 nm because of the n–π* transition, and their fluorescence spectrum showed an emission peak at 450 nm. These results indicate that CDs have been successfully synthesized. A peak at 525 nm is evident in the UV-Vis spectrum, as shown in Fig. S6B,† corresponding to the π–π* electronic transition of the FITC molecule, in which the nanoparticles

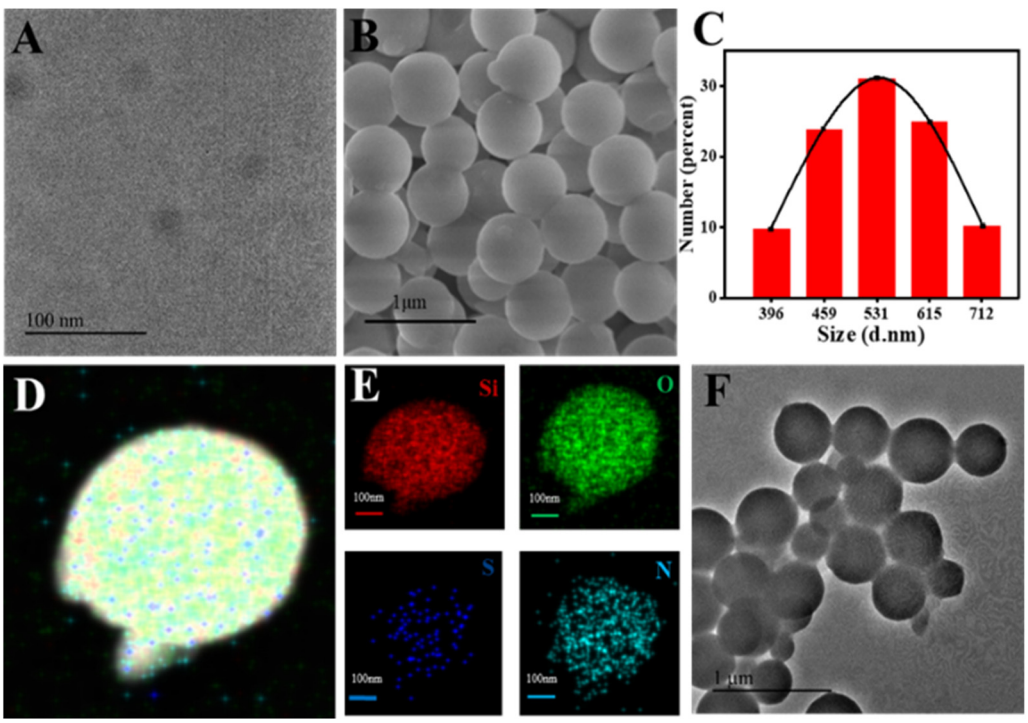

Fig. 3 The TEM image of the synthesized CDs (A), the SEM image of the synthesized FITC-SiO_2 nanocomposites (B), the diameter distributions of the FITC-SiO_2 nanocomposites (C), the HAADF-STEM image of the synthesized FITC-SiO_2 nanocomposites (D), the HAADF-STEM elemental mapping showing the presence of Si, O, S and N (E), and the TEM image of the synthesized CDs-FITC-SiO_2@MIP nanocomposites (F).

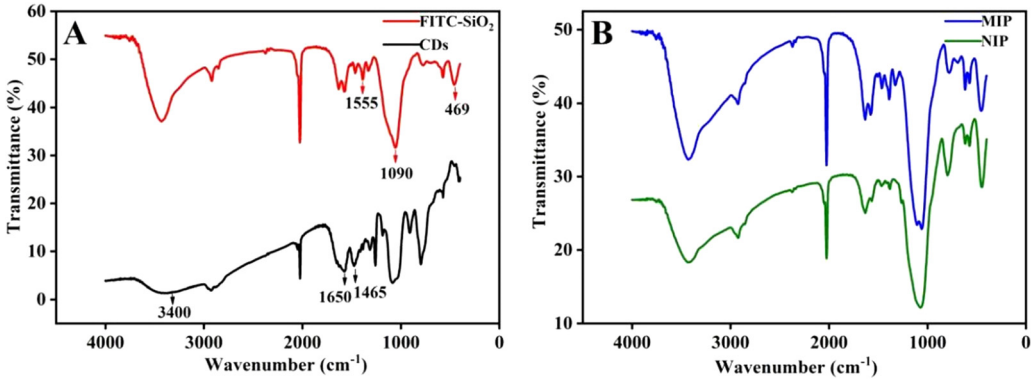

Fig. 4 FTIR spectra of the FITC-SiO_2 nanocomposites (red line) and CDs (black line) (A). FTIR spectra of the CDs-FITC-SiO_2@MIP nanocomposites (blue line) and CDs-FITC-SiO_2@NIP nanocomposites (green line) (B).

becomes wider, probably due to the doping of the FITC molecules in the SiO_2 network structure and their interaction with the Si–OH groups of SiO_2.[43] The fluorescence spectrum of the synthesized FITC-SiO_2 nanocomposites shows an emission peak at 620 nm. These results further show the successful preparation of FITC-SiO_2 nanocomposites. As observable in the FT-IR spectra shown in Fig. 4B, MIP and NIP have similar vibrational peaks, indicating that the template molecule metformin is completely eluted. Moreover, no characteristic peak at 300–400 nm is present in the UV-Vis spectrum of the MIPs (Fig. S7†), implying that the template was successfully removed from the MIPs.

Optimization of MC detection

To obtain good linearity over a short analytical time for the quantitative determination of MCs, various experimental conditions (*viz.* solvent, concentration, temperature, time and synthesis volume ratio of the two fluorescent materials) for synthesizing CDs-FITC-SiO_2@MIP were investigated and optimized. Finally, as the optimal conditions for detecting MCs included the salt solution containing 0.5% NaCl as the solvent, the volume ratio of CDs and FITC-SiO_2 was set as 6 : 1, the amount of CDs-FITC-SiO_2@MIP was fixed at 400 μg mL^{-1}, the adsorption time was selected as 1 min and the adsorption temperature was selected as 25 °C. See ESI SI.2† for details of the optimized conditions.

Analytical performance of the CDs-FITC-SiO_2@MIP sensor

The ratiometric fluorescence detection response of CDs-FITC-SiO_2@MIP was investigated *via* a recognition experiment by introducing different concentrations (0.5, 10, 50, 100, 150, 200, 250, 400, and 500 μg L^{-1}) of MC-RR and MC-LR. It can be observed in Fig. 5A and C that with the increase of MC-RR and MC-LR concentrations under 310 nm excitation, the blue fluorescence intensity of the CDs-FITC-SiO_2@MIP sensor at 450 nm gradually decreased, while the yellow-green fluorescence intensity at 610 nm increased. The images in the inset of Fig. 5A and C show the fluorescence color of the corresponding CDs-FITC-SiO_2@MIP solution after rebinding

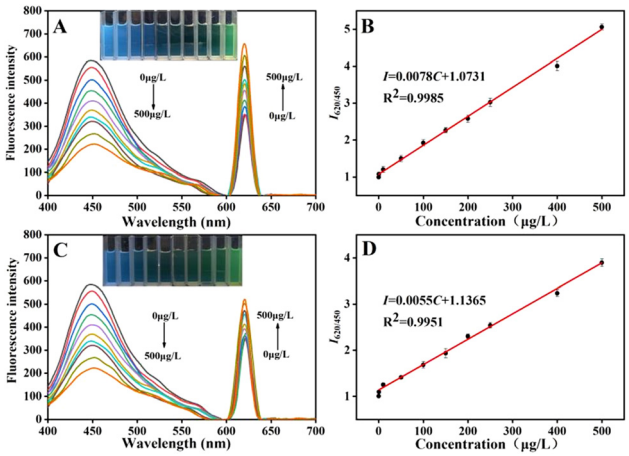

Fig. 5 The fluorescence spectra of the CDs-FITC-SiO_2@MIP solution in response to a series of concentrations: MC-RR (A) and MC-LR (C), and the linear relationships for CDs-FITC-SiO_2@MIP (B and D) (λ_{ex} = 310 nm). The inset shows the images of the fluorescence colors of the corresponding solution under a 365 nm UV lamp. The error bar indicates three individual experiments.

upon adding MC-RR and MC-LR solutions with increased concentrations, respectively, under a 365 nm UV lamp. The color evolution from blue to yellow-green is obvious, making the detection of MCs feasible with the naked eye.

The linear fitting graph for the quantitative analysis of MCs was established based on the fluorescence ratio response value ($I_{620/450}$). As shown in Fig. 5B and D, a linear relationship exists between the $I_{620/450}$ of CDs-FITC-SiO_2@MIP and the concentrations of MC-RR and MC-LR in the 0.5–500 μg L^{-1} range, and the corresponding correlation coefficients (R^2) are 0.9985 and 0.9951, respectively. Therefore, based on the slope of the linear response curve, the LOD of the sensor towards MC-RR and MC-LR was attained down to 0.0132 μg L^{-1} and 0.0223 μg L^{-1} (S/N = 3), respectively.[21] Moreover, the dose response of CDs-FITC-SiO_2@NIP to the MCs has been used to assess the recognition ability of the imprinted memory and specific combination. From Fig. S9A and B,† we can see that the fluo-

rescence intensity did not change significantly with the increase of MCs, owing to the nonspecific recognition and the lack of tailor-made binding sites complementary to the template in construction, size, and functional groups,[44] providing an unremarkable discrepancy between the colors on CDs-FITC-SiO_2@NIP (the inset of Fig. S9A and B†). Therefore, CDs-FITC-SiO_2@MIP exhibited a better recognition response to MCs compared to CDs-FITC-SiO_2@NIP.

The ratiometric fluorescence response signals of MCs, domoic acid, and aflatoxin were investigated to assess the selectivity of CDs-FITC-SiO_2@MIP. Herein, CDs-FITC-SiO_2@NIP, which were synthesized for control purposes, were also reacted with these compounds. The concentration of all compounds was maintained at 500 μg L^{-1} with CDs-FITC-SiO_2@MIP and CDs-FITC-SiO_2@NIP during the interaction. CDs-FITC-SiO_2@NIP showed no obvious ratiometric fluorescence signals upon interaction with the MCs. Besides, CDs-FITC-SiO_2@NIP had no selective reaction to these compounds (MCs, aflatoxin and domoic acid). Contrarily, as shown in Fig. 6A, CDs-FITC-SiO_2@MIP exhibited a good fluorescence response to MC-RR, MC-LR, and MC-YR, because these three MCs contain guanidine structures similar to the dummy template. The CDs-FITC-SiO_2@MIP sensor showed the highest fluorescence ratio for MC-RR among the MCs, because it contains two guanidine groups, while MC-LR and MC-YR contain one guanidine group. Since MC-RR and MC-LR are types of phytotoxins with high content and high toxicity in water, the response of these two kinds of phytotoxins was mainly studied in this paper. The selectivity of CDs-FITC-SiO_2@MIP for different interfering substances was contrasted by calculating the selectivity constant (k), relative selectivity constant (k'), and IF (imprinting factor),[33] as tabulated in Table S2.† As anticipated, the selectivity constant (k) of CDs-FITC-SiO_2@MIP towards MCs (MC-RR, MC-LR, MC-YR and MC-LY) was considerably high. To show the selectivity obtained by the imprinting process, the k' of metformin, indicating the imprinting efficiency, was calculated; it was significantly higher for MCs compared to the other competitive molecules (aflatoxin and domoic acid). The IF value of the MCs was also significantly higher than those of the other competitive compounds. The results show that CDs-FITC-SiO_2@MIP has a selective recognition ability for MCs containing guanidine. Therefore, considering its analytical performance and the obtained selectivity parameters, the CDs-FITC-SiO_2@MIP sensor can be used to detect MCs. In order to further investigate the selectivity of CDs-FITC-SiO_2@MIP, the influence of interfering ions on the detection of MCs was detected by fluorescence methods, and the concentration of MCs was fixed at 500 μg L^{-1}. As shown in Fig. 6B, 10-fold Fe^{3+}, 20-fold Cu^{2+}, 40-fold Al^{3+}, 60-fold Mg^{2+}, 30-fold Zn^{2+}, 80-fold Ca^{2+}, 200-fold Na^{+}, and 200-fold K^{+} had no effect on the fluorescence intensity signals for the determination of MCs (<5%). These results showed that CDs-FITC-SiO_2@MIP has excellent anti-interference capability, indicating that it is a highly selective sensor even in the presence of other common metal ions in the actual water sample. The fluorescence stability of CDs-FITC-SiO_2@MIP was checked by measuring its fluorescence as the response to the concentration variation of MCs up to 50 μg L^{-1} MCs every day while storing at room temperature under subdued light. The change in the fluorescence ratio was monitored for up to 19 days. As evident from Fig. S10,† there was little or no change in the fluorescence ratio of CDs-FITC-SiO_2@MIP after storing until 10 days. However, the fluorescence ratio decreases in the 10–19 day period, but its relative standard deviation (RSD) was 4.81%, still, less than 5%, which indicates that the resultant CDs-FITC-SiO_2@MIP has excellent physical and chemical stability. The change in the fluorescence intensity ratio of CDs-FITC-SiO_2@MIP within 90 min in a 0.5% NaCl solution system is illustrated in Fig. S10.† The fluorescence intensity was recorded at F_{450} and F_{620} every 10 min, and the change in the

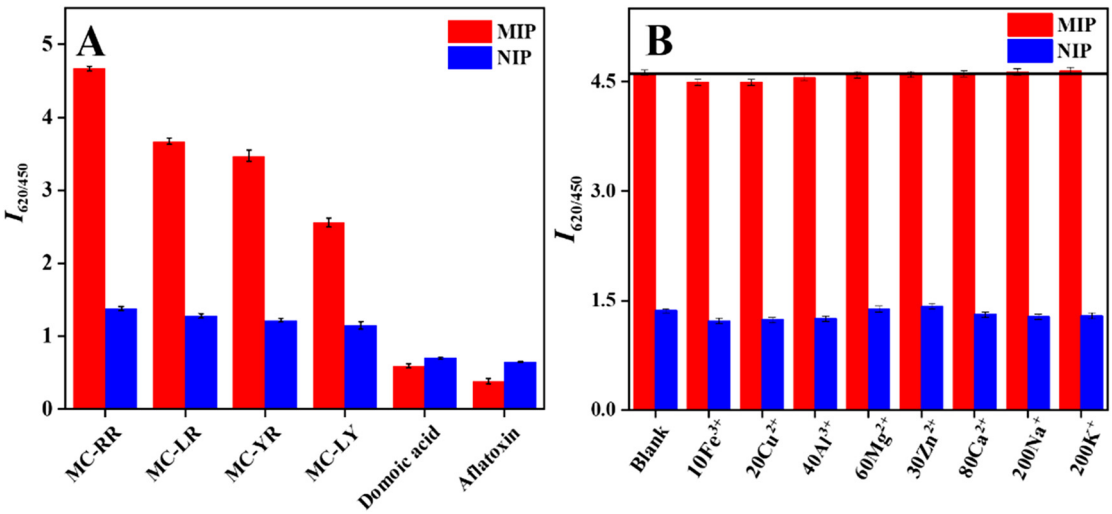

Fig. 6 Selectivity of CDs-FITC-SiO_2@MIP and CDs-FITC-SiO_2@NIP (A). The fluorescence response of CDs-FITC-SiO_2@MIP and CDs-FITC-SiO_2@NIP towards various interfering metal ions (B).

fluorescence intensity ratio of the double emission fluorescence signal was calculated to evaluate the stability of CDs-FITC-SiO_2@MIP. The fluorescence intensity ratio remained relatively stable within 90 min, indicating the good fluorescence stability of the CDs-FITC-SiO_2@MIP sensor during the measurements.

Clustering analysis of MC-RR and MC-LR

The two most common MCs in water are MC-RR and MC-LR,[45] and CDs-FITC-SiO_2@MIP responds to both. Therefore, the cluster analysis method seemed a feasible detection method for MCs. Inspired by the STING algorithm,[46] we took the slope (K) and intercept (b) of the linear fitting graph of the fluorescence ratios corresponding to different molar ratios of MC-RR and MC-LR as two variables for the cluster analysis.

As shown in Fig. 7A, the K and b responses of CDs-FITC-SiO_2@MIP to the linear fitting of the fluorescence ratios corresponding to the different molar ratios of MC-RR and MC-LR were different. MC-RR is dominant when $K > 0.0078$ and $b < 1.074$. However, at $0.0078 < K < 0.0055$ and $1.074 < b < 1.137$, mainly MC-RR and MC-LR dominate, and $K < 0.0055$ and $b > 1.137$ for MC-LR. Further, we explored the change in the K and b responses of CDs-FITC-SiO_2@MIP for the linear fitting of the fluorescence ratios corresponding to the different molar ratios of MC-LR and MC-RR. Fig. 7B presents the linear diagram of the fluorescence ratio of CDs-FITC-SiO_2@MIP in response to the different molar ratios of MC-RR and MC-LR. The fluorescence changes upon mixing MC-RR and MC-LR at the same concentration and equal volume are shown in Fig. S11A† and the linear fitting diagram of the fluorescence ratios is shown in Fig. S11B.† It can be seen that MCs mixed in different molar ratios have different responses to CDs-FITC-SiO_2@MIP (Fig. 7B). As illustrated in Fig. 7B, MC-RR and MC-LR mixed in different molar ratios have a good linear relationship with K. Therefore, the CDs-FITC-SiO_2@MIP sensor is expected to be capable of analyzing different types of MCs in mixed samples.

The analysis of real samples

The practical applicability of the CDs-FITC-SiO_2@MIP sensor was examined by detecting MCs in different water samples such as lake water and tap water. The HPLC-MS method was also used for comparison. Since the matrix seen in different water samples is different, and the matrix will affect the K and b values in the cluster analysis, in order to eliminate the influence of the matrix on the cluster analysis, the water sample was pretreated in this experiment to accurately judge the species and concentration of microcystins. The matrix in lake water was removed through the solid phase extraction experiment to avoid interference, and after that, the water sample was subjected to mass spectrometry (Fig. S12†). The m/z at 995.55 and 519.79 (ref. 47) corresponding to the parent ions of MC-RR and MC-LR were obtained in the mass spectral analysis, proving the existence of MC-RR and MC-LR in Binhai Lake. Moreover, the measured $I_{620/450}$ indicated a linear relationship with the concentrations of MC-RR and MC-LR in Binhai Lake (Fig. S13†). According to the relationship between K and the ratio of MC-RR and MC-LR in the cluster analysis (see Fig. 7B), the proportion of MC-RR and MC-LR in Binhai Lake was 7.9 : 2.1, meaning that the measured lake water mainly contained MC-RR. Hence, MC-RR was used for the labeling experiments in the actual samples. The inset in Fig. 8 shows the fluorescence spectra of the CDs-FITC-SiO_2@MIP sensor in the Binhai Lake water sample with the successive addition of 0, 0.5, 1, and 5 μg L^{-1} MC-RR and the corresponding linear regression curve. The total amount of MCs in Binhai Lake was calculated to be 0.61 μg L^{-1}. According to the ratio measured after removing matrix interference, the concentrations of MC-RR and MC-LR were 0.47 μg L^{-1} and 0.14 μg L^{-1}, respectively. The results of the determination of MCs in the real samples using the CDs-FITC-SiO_2@MIP sensor and those of the HPLC-MS analyses are shown in Table 1. The results obtained by employing the CDs-FITC-SiO_2@MIP sensor were consistent with the HPLC-MS results. The accuracy was further verified by evaluating the recoveries obtained at three

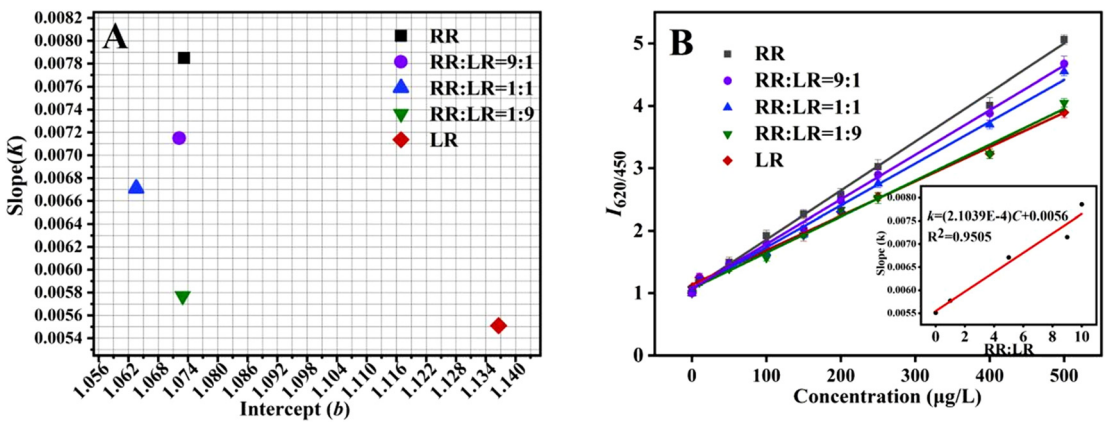

Fig. 7 Cluster analysis diagram of MC-RR and MC-LR at different molar ratios (A), and the linear relationship diagram between MC-RR and MC-LR at different molar ratios and their corresponding fluorescence ratio changes (B). The inset shows the relationship diagram between the different molar ratios of MC-RR and MC-LR with the linear slope.

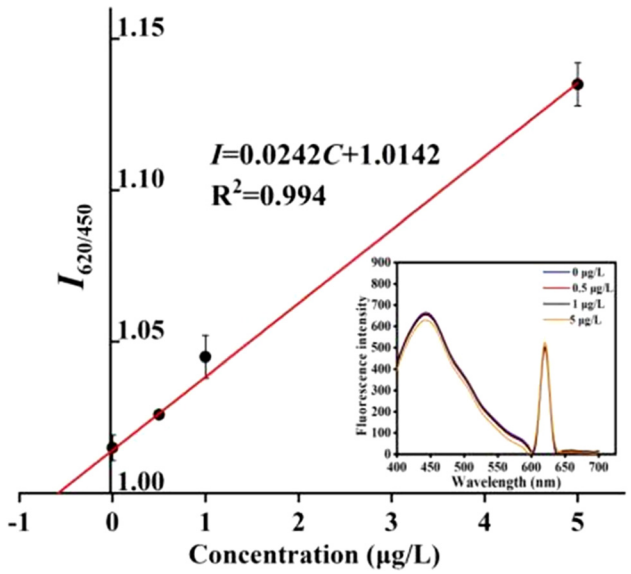

Fig. 8 The plot (n = 3) of change in the fluorescence ratios against different MC-RR concentrations. The inset shows the fluorescence spectra for the determination of MC-RR in the water samples from Binhai Lake by the standard addition method. The concentrations of MC-RR were 0, 0.5, 1, and 5 μg L^{-1}.

Table 1 Comparison of the results of the CDs-FITC-SiO_2@MIP sensor and the results from HPLC-MS for the determination of MCs (n = 3)

Sample		This method (μg L^{-1})	HPLC-MS (μg L^{-1})	RSD (%)
Binhai Lake	MC-RR	0.47	0.50	4.91
	MC-LR	0.14	0.14	4.56
Tap water	MC-RR	0.00	0.00	—
	MC-LR	0.00	0.00	

different concentrations of MC-RR (1, 5, and 20 μg L^{-1}) using the standard addition method (Table S3†). The average recovery of MCs from Binhai Lake water was 104.72–108.14%, while the recovery was 93.15–109.12% in tap water. The relative standard deviation (RSD) ranged from 2.83% to 4.91%. It shows the potential for the monitoring of MCs in environmental water without the need for sophisticated analytical instruments. Besides, the current analytical methods and products applicable to the determination of MCs in water were compared (Table S4†). The linear range and LOD in this study were comparable with those obtained in previous studies.

Conclusions

In summary, we have constructed an innovative composite nanoscale molecule-imprinted ratiometric fluorescence sensor (CDs-FITC-SiO_2@MIP) for specific recognition and sensitive visual detection of MCs. Metformin was used as a dummy template for CDs-FITC-SiO_2@MIP synthesis, and the fluorescence sensing method of MCs was successfully established and confirmed. The ratio of fluorescence quenching to fluorescence enhancement of CDs-FITC-SiO_2@MIP was proportional to the concentration of MCs, enabling the successful detection of MCs in environmental water by the ratiometric fluorescence method. It was observed that different concentrations of MCs could change the color of CDs-FITC-SiO_2@MIP, making the sensor capable of semi-quantitative determination of MCs by the naked eye. Through cluster analysis experiments, the sensor could analyze the types of MCs present in actual samples and detect different kinds of MCs. We successfully detected two microcystins in this study, which provides a direction for the sensitive detection of multiple components. Hence, we expect that our work will inspire the development of effective sensors for detecting MCs and provide a potential platform for determining other toxic substances in the future.

Author contributions

Ping Li: conceptualization, methodology, writing – original draft, formal analysis and data curation. Hao Fu: investigation, data curation, and writing – review and editing. Zhenyu Bai: supervision, validation, and writing – review and editing. Xiaoyang Feng: validation and writing – review and editing. Ji Qi: visualization and writing – review and editing. Xingliang Song: project administration, funding acquisition, methodology, and resources. Xueping Hu: project administration, funding acquisition, methodology, and resources. Lingxin Chen: visualization and writing – review and editing.

Conflicts of interest

There are no conflicts to declare.

Acknowledgements

This work was financially supported by the National Natural Science Foundation of China (21906075); the Natural Science Foundation of Shandong Province (ZR2020MD077); the Key Research and Development Program of Linyi City (2020ZX007).

References

1 K. Westphal, D. Graeber and A. Musolff, *Sci. Total Environ.*, 2019, **667**, 769–779.
2 W. A. Hassanain, E. L. Izake, M. S. Schmidt and G. A. Ayoko, *Biosens. Bioelectron.*, 2017, **91**, 664–672.
3 S. Rezaitabar, A. E. Sari, N. Bahramifar and Z. Ramezanpour, *Sci. Total Environ.*, 2017, **575**, 1130–1138.
4 B. C. Hitzfeld, S. J. Hoger and D. R. Dietrich, *Environ. Health Perspect*, 2000, **108**, 113–122.
5 K. I. Harada, K. Tsuji, M. F. Watanabe and F. Kondo, *Phycologia*, 1996, **35**, 83–88.

6 L. Chen, J. P. Giesy and P. Xie, *Sci. Total Environ.*, 2018, **621**, 649–653.
7 H. Thuret-Benoist, V. Pallier and G. Feuillade-Cathalifaud, *Environ. Toxicol. Pharmacol.*, 2019, **72**, 103223.
8 L. Reverté, D. Garibo, C. Flores, J. Diogène, J. Caixach and M. Campàs, *Environ. Sci. Technol.*, 2013, **47**(1), 471–478.
9 J. J. Zhang, T. F. Kang, Y. C. Hao, L. P. Lu and S. Y. Cheng, *Sens. Actuators, B*, 2015, **214**, 117–123.
10 D. W. Marsan, S. M. Conrad, W. L. Stutts and C. H. Parker, *Heliyon*, 2018, **4**(3), e00573.
11 A. Sassolas, G. Catanante, D. Fournier and J. L. Marty, *Talanta*, 2011, **85**(5), 2498–2503.
12 B. Zheng, H. Fu, J. P. Berry and B. McCord, *J. Chromatogr. A*, 2016, **1431**, 205–214.
13 R. A. Halvorson, W. Leng and P. J. Vikesland, *Anal. Chem.*, 2011, **83**(24), 9273–9280.
14 S. M. Taghdisi, M. Danesh, M. Ramezani, N. S. Ghows, A. M. Shaegh and K. Abnous, *Talanta*, 2017, **166**, 187–192.
15 Z. Song, Y. Song, Y. Wang, J. Liu, Y. Wang and W. Lin, *Talanta*, 2022, **239**, 123115.
16 L. Chen, X. Wang and W. Lu, *Chem. Soc. Rev.*, 2016, **45**(8), 2137–2211.
17 Z. Qi, R. Lu, S. Wang, C. Xiang, C. Xie and M. Zheng, *Microchem. J.*, 2021, **161**, 105798.
18 L. He, L. Liu, C. G. Lin, J. M. Ruan, X. M. Liang, Y. Zhou and L. L. Wei, *Fish Physiol. Biochem.*, 2005, **46**, 2005–2014.
19 E. A. Mbukwa, T. A. Msagati and B. B. Mamba, *Anal. Bioanal. Chem.*, 2013, **405**(12), 4253–4267.
20 Y. Li, J. You, Y. He, Y. Ge, G. Song and J. Zhou, *ChemistrySelect*, 2020, **5**(38), 12028–12033.
21 X. Wang, J. Yu, X. Wu, J. Fu, Q. Kang, D. Shen and L. Chen, *Biosens. Bioelectron.*, 2016, **81**, 438–444.
22 J. He, X. Jiang, P. Ling, J. Sun and F. Gao, *ACS Omega*, 2019, **4**(5), 8282–8289.
23 M. Wang, N. Li, S. Wang, J. Chen and X. Su, *Sens. Actuators, B*, 2021, 130430.
24 Y. Cui, W. Duan, Y. Jin, F. Wo and J. Wu, *ACS Sens.*, 2020, **5**(7), 2096–2105.
25 Y. Yan, J. Sun, K. Zhang, H. Zhu, H. Yu, M. Sun and S. Wang, *Anal. Chem.*, 2015, **87**(4), 2087–2093.
26 C. Zou, M. F. Foda, X. Tan, K. Shao, L. Wu, Z. Lu and H. Han, *Anal. Chem.*, 2016, 7395.
27 C. Aimin, P. Xiao, P. Zaifa, S. Kang, W. Jing and F. Maohong, *J. Agric. Food Chem.*, 2018, **66**(25), 6431.
28 M. Li, H. Liu and X. Ren, *Biosens. Bioelectron.*, 2017, **89**, 899–905.
29 X. Wang, S. Yu, W. Liu, L. Fu, Y. Wang and J. Li, *ACS Sens.*, 2018, **3**(2), 378–385.
30 W. He, R. Gui, H. Jin, B. Wang and Y. Fu, *Talanta*, 2018, **178**, 109–115.
31 G. Liu, Z. Chen, X. Jiang, D. Q. Feng, J. Zhao and D. Fan, *Sens. Actuators, B*, 2016, **228**, 302–307.
32 S. Su, L. Lin, H. Li, X. Wen, R. Yan and C. Tao, *Microporous Mesoporous Mater.*, 2022, **330**, 1387–1811.
33 W. Stober and A. Fink, *J. Colloid Interface Sci.*, 1968, **26**, 62–69.
34 R. Zhu, M. Lai, M. Zhu, H. Liang, Q. Zhou and R. Li, *Spectrochim. Acta, Part A*, 2021, **244**, 118845.
35 E. Özgür, H. K. Patra, A. P. F. Turner, A. Denizli and L. Uzun, *Ind. Eng. Chem. Res.*, 2020, **59**(36), 16068–16076.
36 J. Sun, W. Li, Y. Hou, X. Zhang, Z. Gao and B. Wang, *ACS Omega*, 2021, **6**(42), 28356–28365.
37 A. Burger, H. N. Le, J. Brazard, G. Barnoin, S. Vincent, B. Michel and J. Leonard, *Chem. – Eur. J.*, 2021, **27**(4), 1364–1373.
38 K. Wei, L. Zhang, S. L. Jiang and Q. Zhang, *Chin. J. Chem. Phys.*, 2019, **32**(6), 643–648.
39 X. Wang, S. Yu, J. Wang, J. Yu, M. Arabi and L. Fu, *Talanta*, 2020, **211**, 120727.
40 F. You, Y. F. Zhou and X. E. Zhang, *Anal. Chem.*, 2006, **78**(20), 7138–7144.
41 H. Sunayama and T. Takeuchi, *ACS Appl. Mater. Interfaces*, 2014, **6**(22), 20003–20009.
42 X. Du and J. He, *Langmuir*, 2011, **27**(6), 2972–2979.
43 T. A. Taton, C. A. Mirkin and R. L. Letsinger, *Science*, 2000, **289**(5485), 1757–1760.
44 S. Xu and H. Lu, *Biosens. Bioelectron.*, 2015, **73**, 160–166.
45 E. M. Janssen, *Water Res.*, 2019, **151**, 488–499.
46 W. Wang, J. Yang and R. Muntz, C., In: Proceedings of the 23th VLDB Conference, 1997, 186–195.
47 V. Ríos, I. Moreno, A. I. Prieto, M. Puerto, D. Gutiérrez-Praena, M. E. Soria-Díaz and A. M. Cameán, *Food Chem. Toxicol.*, 2013, **57**, 170–178.